INSTITUTE OF PHYSICS PUBLISHING JOURNAL OF PHYSICS: CONDENSED MATTER

J. Phys.: Condens. Matter **18** (2006) S1151–S1176 doi:10.1088/0953-8984/18/28/S04

A practical guide to giant vesicles. Probing the membrane nanoregime via optical microscopy

Rumiana Dimova[1], **Said Aranda, Natalya Bezlyepkina, Vesselin Nikolov**[2], **Karin A Riske**[3] **and Reinhard Lipowsky**

Max Planck Institute of Colloids and Interfaces, 14424 Potsdam, Germany[4]

E-mail: Rumiana.Dimova@mpikg.mpg.de

Received 3 January 2006
Published 28 June 2006
Online at stacks.iop.org/JPhysCM/18/S1151

Abstract
Research on giant vesicles is becoming increasingly popular. Giant vesicles provide model biomembrane systems for systematic measurements of mechanical and rheological properties of bilayers as a function of membrane composition and temperature, as well as hydrodynamic interactions. Membrane response to external factors (for example electric fields, ions and amphiphilic molecules) can be directly visualized under the microscope. In this paper we review our current understanding of lipid bilayers as obtained from studies on giant unilamellar vesicles. Because research on giant vesicles increasingly attracts the interest of scientists from various backgrounds, we also try to provide a concise introduction for newcomers in the field. Finally, we summarize some recent developments on curvature effects induced by polymers, domain formation in membranes and shape transitions induced by electric fields.

(Some figures in this article are in colour only in the electronic version)

1. Introduction

Cells, being the basic building units of most living creatures, are the obvious object of interest when properties and functions of organisms are to be deduced. The autonomy of a cell is ensured by a bounding membrane. Indeed, every living cell on this planet has some type of membrane. Studying the major characteristics of the plasma membrane and other intracellular membranes is the foundation of modern cellular biology. However, because all scientific fields

[1] Author to whom any correspondence should be addressed.
[2] Present address: Department of Materials Science and Engineering, Johns Hopkins University, Baltimore, MD, USA.
[3] Present address: Instituto de Física da Universidade de São Paulo, São Paulo, Brazil.
[4] http://www.mpikg.mpg.de/th

are interrelated and mutually complementary irrespective of their inherent diversity, membranes are an object of study in many other disciplines (biochemistry, biophysics, colloid chemistry, etc), which implies different approaches of analysis. The links between membrane physics and other areas of research are becoming increasingly evident and important. As a result, the field of membrane structure and characteristics is attracting the attention of a growing number of researchers.

Biological membranes are highly organized bilayer assemblies, measuring a few nanometres in thickness. Phospholipids are their major compounds. The type of structure formed by the phospholipids generally depends on the water/lipid ratio and the temperature of the media. At relatively low concentrations, the molecules assemble in bilayers whose thickness is of the order of 4 nm, but in the lateral direction they may extend up to millimetres. The phospholipid bilayer is the major component of virtually all biological membranes and it is with the bilayer that the study of a membrane logically begins.

Vesicles are membrane 'bubbles' formed by bending and closing up a lipid bilayer. Various experimental techniques have been developed for preparing liposomes of different size (from nanometres to tens of microns). The largest (several tens of microns) are called 'giant' vesicles and are an extraordinarily convenient system for studying the membrane behaviour. They are well visible under an optical microscope and thus allow for direct manipulation and observation of membrane interactions. In contrast, working with conventional vesicles (a few hundreds of nanometres) usually involves the application of indirect methods and techniques for observation. In addition, their small sizes often raise questions about effects due to membrane curvature when molecular interactions are considered. In contrast, the giant vesicles that have a size in the micrometre range, i.e. are of cell-size, reflect the membrane properties and behaviour as they are in cells.

Thus, giant unilamellar vesicles (GUVs) are a very practical tool for studying membrane properties. In addition, the possibility to directly visualize certain interactions in a small but optically resolvable volume (about ten picolitres) encapsulated by the vesicle membrane has provoked the development of various ideas from interdisciplinary fields. To mention a few recent ones, giant vesicles have been considered as (i) a possible construct of microreactors (Noireaux and Libchaber 2004, Fischer *et al* 2002, Michel *et al* 2004); (ii) a means to study microcompartmentation and cellular crowding (Helfrich *et al* 2002, Long *et al* 2005); (iii) microscopic vessels for protein crystallization (Yamashita *et al* 2002). In addition the recent finding that certain amphiphilic diblock copolymers can form giant vesicles, or polymersomes (Discher *et al* 1999), has reinforced work related to development of drug delivery tools. The main application of GUVs, though, remains the characterization of the mechanical and rheological properties of single- or multi-component membranes as well as investigation of bilayer interactions.

It is the object of this paper to review the knowledge on lipid bilayers as obtained from studies on giant unilamellar vesicles. The presented material is far from being exhaustive and covers certainly a subjective selection of recent work in the field, unavoidably omitting some important papers. However, because studies on giant vesicles increasingly attract the interest of scientists from various backgrounds and different scientific domains, with this review we aim to provide a concise 'start-up package' of knowledge for newcomers. At the same time, for the audience with experience on giant vesicles, we summarize recent developments, emphasize aspects which are sometimes overlooked, and raise open questions in the field.

The work is organized as follows. In the next section we summarize the types of deformation modes of model membranes and give typical values of the material parameters characterizing the membrane response to various constraints. Then, the features of the two main protocols for vesicle formation are summarized. In two subsequent sections we present

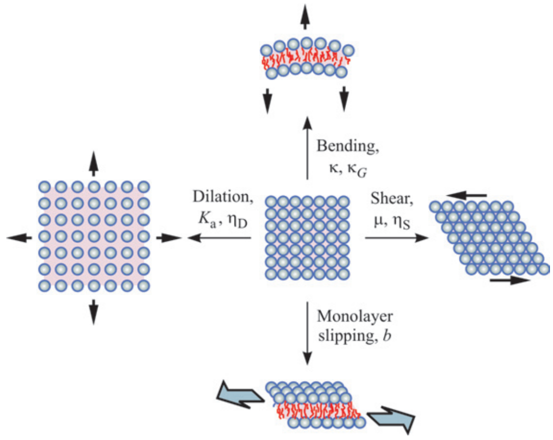

Figure 1. Schematic presentation of some classical modes of bilayer deformations: dilation, bending, shear, monolayer slipping; and the constants characterizing the membrane response to these deformations.

methods developed for measuring the elastic and rheological properties of membranes, both in the fluid and in the gel phase. The membrane response to external perturbation (e.g. inserting molecules, electric fields) is discussed in terms of vesicle deformation and mechanical strength. Overall, our paper discusses vesicles both in inert solutions and in the presence of molecules interacting with the membrane. An example for addressing ion–membrane interactions is given in the concluding section.

2. Classical modes of deformations

When considering vesicles from one preparation sample two types of features are to be distinguished: (i) the collective or batch properties are characteristic for every vesicle in the sample and depend mainly on the membrane thermodynamic state and composition, for example, collective properties are the bending rigidity, stretching elasticity and membrane viscosity; (ii) individual properties which are particular for every vesicle are, for instance, its geometrical parameters or shape and spontaneous curvature.

2.1. Batch properties

From observations on giant vesicles and their response to different perturbations one may in principle deduce the mechanical and rheological properties of their membranes. Simplistically, the lipid bilayer may be viewed as a single film or slab, or in other words, one may ignore the presence of two distinct monolayers. However, this simplification is inappropriate when bending elasticity is concerned. Mechanically this film may be curved, compressed or dilated, and sheared. In the equilibrium state and within the linear limit, the membrane responses to various constraints are characterized by the following constants: bending rigidity, κ, Gaussian curvature modulus, κ_G, area compressibility modulus, K_a, and shear elastic modulus, μ; see figure 1.

At physiological temperatures most lipid membranes are fluid; therefore $\mu = 0$. Below the phase transition temperature of the lipids, single-component membranes crystallize. Mechanically, the bilayer acquires a non-zero shear elasticity ($\mu \neq 0$). In this so-called 'gel' phase (see section 5), the relative motion of membrane inclusions is principally hindered. The

Table 1. Some typical values for the characteristics of lipid membranes in fluid and gel phase, and for polymersome bilayers.

	Lipid membrane in the fluid phase	Lipid membrane in the gel phase	Polymer membrane[a]
Bending rigidity, κ	0.9×10^{-12} erg ($\sim 20\, k_B T$) (for κ-values of different lipid bilayers see e.g. Seifert and Lipowsky 1995 and Rawicz *et al* 2000)	14×10^{-12} erg ($\sim 350\, k_B T$)[b] (Dimova *et al* 2000b Mecke *et al* 2003)	1.4×10^{-12} erg ($\sim 35\, k_B T$) (Discher *et al* 1999) 1.7×10^{-12} erg ($\sim 42\, k_B T$) (Dimova *et al* 2002b)
Stretching elasticity, K_a	240 dyn cm^{-1}, see e.g. (Rawicz *et al* 2000)	$\sim$300 dyn cm^{-1} (Needham and Evans 1988)	120 dyn cm^{-1} (Discher *et al* 1999) 470 dyn cm^{-1} (Dimova *et al* 2002b)
Shear surface viscosity, η_S	$\sim 5 \times 10^{-6}$ dyn s cm^{-1} (Dimova *et al* 1999)	Diverges (Dimova *et al* 2000b)	$\sim 2 \times 10^{-3}$ dyn s cm^{-1} (Dimova *et al* 2002b)
Dilatational surface viscosity, η_D	5×10^{-3} dyn s cm^{-1} (Sandre *et al* 1999) or 3.5×10^{-4} dyn s cm^{-1}[c] (Brochard-Wyart *et al* 2000)	—	—
Intermonolayer slip, b	10^6–10^7 dyn s cm^{-3} (Merkel *et al* 1989)	— —	1.3×10^8 dyn s cm^{-3} (Dimova *et al* 2002b)

[a] The values reported for polymersomes depend on the type of diblock copolymer used and vary in different references.
[b] This value corresponds to the bending rigidity of membranes at temperatures about 5° below the main phase transition temperature of the lipid.
[c] Both values for η_D have been reported by the same group. Presumably the second is the better estimate.

fluidity of the membrane at higher temperatures is essential in the case of cellular membranes because it permits the displacement of membrane anchored macromolecules or inclusions, for example trans-membrane proteins. The membrane, on the one hand, and the surrounding fluid, on the other, impose a hydrodynamic drag to the motion of an inclusion (see section 5.2). The resistance or shear in the plane of the film is characterized by the shear viscosity, η_S. One may equivalently define a viscosity η_D related to the dilation and compression of the membrane. For a complete and realistic description of the membrane dynamics one has to explicitly account for the existence of the membrane constitutive parts: two monolayers which may slip with respect to each other; see figure 1. To this motion, the membrane opposes with a friction force the amplitude of which is proportional to the coefficient of 'intermonolayer friction', b. Generally, all the constants listed above are defined in the zero frequency and infinite size limits. In other words, they are supposed constant in time and homogeneous in space in the scale of the structural details of the system. In table 1 we have given some typical values of these constants for both the fluid phase and the gel phase of the membrane. In the gel phase, the membrane viscosity diverges and the bending rigidity drastically increases. For comparison we have given some known values of these constants for polymersomes. In this latter case, depending on the molecular weight of the diblock copolymer used, the membrane thickness can be a few times larger than the one of the lipid membranes. As a result the mechanical properties of the polymer membrane depend on the length of the hydrophobic segment of the polymers (Aranda-Espinoza *et al* 2001).

2.2. *Properties of individual vesicles*

Apart from the intermonolayer slip, the bilayer nature of membranes is reflected also in the so-called spontaneous curvature. In the case of an asymmetry between the compositions of

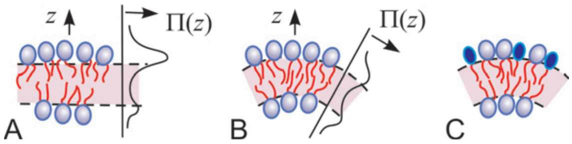

Figure 2. Origins of membrane spontaneous curvature. (A) The difference in the number of molecules composing each monolayer increases the lateral pressure, $\Pi(z)$, in the monolayer with more molecules. This defines a preferred (spontaneous) curvature which leads to a partial release of the lateral pressure frustration in the headgroup area (B). A similar effect can be expected when guest molecules are asymmetrically inserted (C); see also section 4.2.

the two constituent leaflets there is a preferred direction in which the membrane would curve. This composition asymmetry can be due to the different number or geometry of the molecules constituting each monolayer, as illustrated in figure 2. The gradient of the lateral pressure across the membrane in the direction normal to the membrane as schematically shown creates an intrinsic bending moment. Curving the membrane results in release of the pressure in the headgroup area (compare figures 2(A) and (B)). Flip-flop of molecules across the membrane also leads to the same effect, but lipid flip-flop times are usually very long (of the order of several hours (Kornberg and Mc Connell 1971)). Thus, depending on the preparation history every vesicle can have its own effective spontaneous curvature. This leads to a rich variety of experimentally observable shapes, such as prolates, oblates, stomatocytes, vesicles of higher genus (i.e. vesicles with handles) (Lipowsky 1991, Mutz and Bensimon 1991, Wintz *et al* 1996, Haluska *et al* 2002). In the absence of flip-flops between the two monolayers these shapes (excluding those of higher genus) can be systemized into a morphological phase diagram (Seifert 1997, Döbereiner *et al* 1997, Döbereiner 2000) according to the vesicle spontaneous curvature (area difference between the two monolayers) and its reduced volume, v. The latter is defined as the ratio between the vesicle volume, V, and the volume of a sphere of area equal to the vesicle area, A:

$$v = \frac{3\sqrt{4\pi}\,V}{A^{3/2}}. \tag{1}$$

Introducing the reduced volume as a parameter is a convenient way of characterizing the excess vesicle area available for fluctuations and shape transformation away from a sphere. The values v can take are $\leqslant 1$. For $v = 1$ the vesicle is a sphere. For $v < 1$ the vesicle has excess area.

When changes in the spontaneous curvature are concerned, one should distinguish local and global contributions; see (Lipowsky 1999). The global contribution to the spontaneous curvature arises if the number of molecules within the two monolayers is conserved, i.e., it is constant on the time scales of the experiment. Thus, this global contribution arises in the absence of flip-flops. This is a good assumption for pure lipid bilayers but not, in general, for multicomponent bilayers. Cholesterol, for example, undergoes frequent flip-flops on the scale of seconds.

3. Preparation and observation of giant vesicles

3.1. Two preparation protocols

There are two widely used techniques for vesicle formation. One is based on the effect of electric fields, or electroswelling, and the other is spontaneous swelling (or gentle hydration). A number of modified procedures for preparing giant vesicles have been reported but it would take us too far to give a detailed review on them. Instead, in table 2, we give a short summary and some typical features of the two protocols.

Table 2. Characteristic features of two protocols for formation of giant unilamellar vesicles. The methods are applicable to forming both liposomes and polymersomes.

	Electroformation	Spontaneous swelling
Substrate for vesicle growing	Glass plates covered with indium tin oxide (ITO) or Platinum wires of diameter ~0.5 mm (inter-electrode spacing ~2 mm)	Glass surface or Teflon plate (roughened with sand paper)
Lipid concentration	Typically 1–2 mg ml^{-1} lipid in organic solvent	Typically 10 mg ml^{-1} lipid in organic solvent
Pre-swelling stage	None or Weak AC field (~0.5 V, 10 Hz)	Pre-hydration in atmosphere saturated with water (can be achieved with a water bath or a flow of nitrogen saturated with water vapour)
Growing time	Few hours: the electric field is gradually increased to about 1.5–2 V (for inter-electrode spacing of ~2 mm) in 0.5 V steps every 20 min; at the end the AC field frequency is reduced to 5 Hz and applied for several minutes which helps for detaching the vesicles from the electrodes.	1–3 days: a typical cloud (1–2 mm in diameter) of vesicle suspension is formed. One should avoid shaking the solution otherwise the cloud disperses and harvesting the vesicles is significantly hindered.
Typical vesicle size and characteristics	20–50 μm in size, spherical, often unilamellar, tense	5–20 μm, deflated, very polydisperse in size, often multilamellar and with defects
Introducing reference	Angelova and Dimitrov (1986); Angelova *et al* (1992)	Reeves and Dowben (1969); Needham and Evans (1988)
General remarks	The vesicles are to be formed at a temperature above the main phase transition temperature of the lipid To prevent bacteria development in the formation chamber, one can add 0.1 mM NaN_3	

The vesicle preparation procedure starts with spreading a lipid solution on a substrate on which the vesicles are to be formed. The lipids are usually dissolved in pure chloroform or a mixture of solvents (e.g. chloroform and less hydrophobic solvents like methanol). The choice for a solvent depends on the lipid architecture or the substrate hydrophobicity. The substrate is then left for several hours under vacuum for removal of the organic solvent. After a pre-swelling stage (see table 2) water or buffer is introduced into the swelling chamber containing the substrate. This is the final preparation step in the spontaneous swelling procedure. Within a couple of days, a typical cloud (1–2 mm in size) is formed in the flask pending above the substrate and it can be harvested with a pipette. In the case of electroformation, the vesicle swelling is accelerated by applying an AC field (see table 2). In suitably assembled chambers it is possible to directly observe the vesicle formation process under the microscope which is, in general, not the case for the spontaneous swelling method. In a few hours (or several minutes in the case of polymersomes) the vesicles are formed. In both cases, the population of vesicles is far from being monodisperse in size. In addition, the vesicles are interconnected with thin membrane tubes or 'tethers', and one should be aware of possible exchange of lipids among neighbouring vesicles and/or the substrate. The best model vesicles are usually considered to

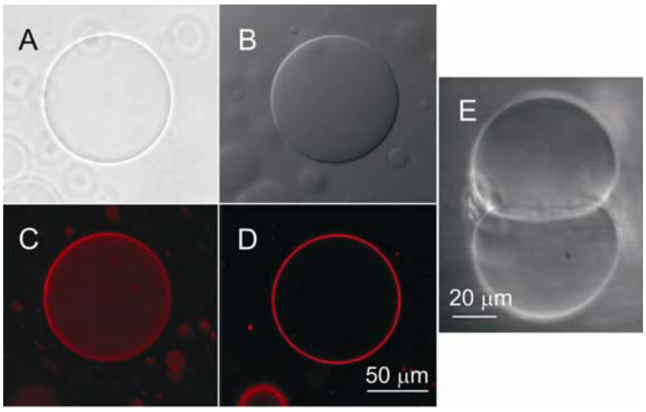

Figure 3. Microscopy observation of giant vesicles. (A)–(D) A giant lipid vesicle observed from above using three different microscopy techniques: (A) phase contrast; (B) differential interference contrast; ((C), (D)) confocal microscopy, where (C) is a projection averaged image and (D) is an equatorial section image. (E) Side view of a vesicle sitting on a glass surface and its mirror projection (phase contrast microscopy). The vesicle is filled with sucrose and is in a glucose environment at osmolarity 200 mOsm g^{-1}. The effect of gravity deforming the vesicle is visible from the snapshot.

be those that are not connected to others, do not have internal formations, and their membrane is smooth and without defects. In some cases, excess area (i.e. small reduced volume) is also an advantage, for example when membrane fluctuations are analysed. Thus, perfect vesicles are, in general, hard to find. The electroswelling procedure usually leads to spherical vesicles (with reduced volume $v = 1$) while vesicles formed by spontaneous swelling are found to adopt a surprisingly large variety of shapes ($v < 1$).

Both of these procedures have been applied to the formation of lipid vesicles as well as polymersomes (Discher *et al* 1999, Dimova *et al* 2002b). Because of the extremely high membrane viscosity of the polymersomes (see table 1), using the procedure of spontaneous swelling requires much longer times. On the other hand, because these membranes are relatively tough (Aranda-Espinoza *et al* 2001), one can apply higher voltages in the electroswelling procedure which accelerates the vesicle formation time.

Both protocols have advantages and disadvantages. The electroformation procedure is faster and the vesicles are usually larger, unilamellar and with fewer defects, but they are initially tense. Apart from that, the electroswelling procedure is not suitable for growing vesicles in the presence of salt, while spontaneous swelling of giant vesicles can be successful at physiological conditions, e.g. at ∼100 mM NaCl (Akashi *et al* 1996). Recently, there have also been a few reports on vesicle formation under conditions of high ionic strength (Yamashita *et al* 2002, Estes and Mayer 2005).

3.2. Light microscopy of giant vesicles

Giant vesicles can be directly observed with conventional light microscopy techniques like phase contrast microscopy and differential interference contrast microscopy (DIC); see figures 3(A) and (B). Even though the lipid membrane thickness (about 4 nm) is much below the optical microscope resolution limit (about half a micron) the vesicles can be visualized due to a difference between the membrane and solution refractive indices or a phase shift in the diffracted light. A commonly used trick for enhancing the image obtained with phase contrast microscopy is to use diffraction index asymmetry of the solutions inside and outside the vesicles. To achieve this, the vesicles are swollen in sucrose solution and subsequently diluted (3–5 times) in glucose (typical concentrations are 100–200 mM). The two solutions have to be isotonic to prevent the vesicles from collapsing, i.e. bursting or shrinking because of the osmotic difference across the membrane. Achieved in this way, the diffraction index asymmetry makes the vesicles look dark on a lighter background when observed under phase contrast (see figure 3(A)) or gives them an artificial 'shadowing' when observed with DIC (see figure 3(B)). The three-dimensional appearance in the latter case does not represent the true geometric nature of the vesicles and cannot be applied for accurate measurement of actual heights and depths (Davidson and Abramowitz 1999).

In addition to enhancing the optical contrast, the dilution of the vesicles helps disperse them from the clusters in which they are initially formed, and at least partially break the thin membrane tubes ('tethers') interconnecting individual vesicles. In addition, the sugar asymmetry makes the vesicles heavier and thus easier to locate at the bottom of the observation chamber. The density difference, $\Delta\rho$, between sucrose and glucose solutions of osmolarity 200 mOsm g^{-1} is approximately 1.05×10^{-2} g cm^{-3}. Using higher sugar concentrations enhances the optical contrast and facilitates the observations even more. However, one should be aware that at high density differences, i.e. higher sugar concentrations, gravity effects are present. For example, the vesicle may be deformed (Kraus *et al* 1995) and its fluctuation spectra influenced (Döbereiner *et al* 1997). Henriksen and Ipsen (2002) suggested a gravity criterion which can be used to estimate the density difference, $\Delta\rho_{max}$, below which the effect of gravity on fluctuation spectroscopy measurements is negligible. Neglecting the effect of the vesicle spontaneous curvature, this criterion can be presented as

$$\Delta\rho_{max} \leqslant \frac{12\kappa/R^2 + \sigma}{gR^2} \tag{2}$$

where R is the vesicle radius, σ is the membrane tension and g is the acceleration of gravity. For example, for a floppy vesicle ($\sigma \sim 2 \times 10^{-5}$ dyn cm^{-1}) of radius about 20 μm, gravity would have an effect at density differences of the glucose/sucrose solutions larger than about 5 g l^{-1}, which corresponds to osmolarity ~100 mOsm g^{-1}. But for vesicles at the same osmolarity conditions but of slightly larger radius, gravity would have a considerable effect on their fluctuation spectrum and, at higher osmolarities, the vesicles can be further deformed; see figure 3(E).

When the starting lipid solution in organic solvent has been prepared to contain a small amount of fluorescent lipid (in general less than about 1 mol%) the vesicle membrane can be observed with fluorescent and confocal microscopy. Fluorescence images often reveal vesicle 'defects' which are not detectable under phase contrast or DIC because of their thin structure (Rodriguez *et al* 2005). The fluorescent molecules employed can also be water soluble and encapsulated in the vesicle interior, which allows for performing content mixing essays; see e.g. (Heuvingh *et al* 2004). Although fluorescence microscopy can reveal more details of the vesicle, it is a technique which requires longer time for the image acquisition (~0.5 s/image) and is not suitable for recording fast events. Additional care has to be taken if one wants to prevent dye bleaching.

There are a few other techniques based on optical microscopy that have been applied to the observation of giant vesicles. One of them is the reflection interference contrast microscopy (introduced in Rädler and Sackmann (1993)) which has a nanometre precision in the vertical direction and can resolve the position of a vesicle membrane within a thin slab (a few micrometres in thickness) close to a glass surface. Another more exotic approach of vesicle observation involves tilting of the whole microscope under an angle of 90° so that the side view of a vesicle sitting on a surface can be observed applying phase contrast, DIC or fluorescence microscopy (Abkarian *et al* 2001, Abkarian and Viallat 2005). One example of a phase contrast snapshot of a vesicle resting on a glass substrate is given in figure 3(E). The mirror reflection of the vesicle is also visible. Recently, the side view detection and contour analysis were found to provide a non-destructive and direct method for extracting simultaneously the bending rigidity of the membrane and the adhesion strength to the substrate (Gruhn *et al* 2006).

4. Elastic properties of membranes deduced from measurements on giant vesicles

4.1. Bending rigidity, stretching elasticity and spontaneous curvature measurements

At room temperature, most lipid membranes are soft and flexible. The energy needed to bend a membrane is of the order of ten k_BT, where k_B is the Boltzmann constant and T is temperature (see table 1). Because membranes can be considered as being made of two parallel elastic sheets, the stretching elasticity modulus of lipid membranes, K_a, can be approximately estimated using the expression (see e.g. (Boal 2002))

$$K_a = \alpha\kappa/h^2 \tag{3}$$

where h is the membrane thickness and α is a numerical constant. A polymer brush model combined with experimental measurements yields $\alpha = 24$ (see Rawicz *et al* 2000, but note that there h is not exactly the membrane thickness as defined here). In contrast, molecular dynamics simulations lead to $\alpha \cong 48$, in agreement with a simple model based on classical elasticity theory (Goetz *et al* 1999). Measuring the bending rigidity κ for membranes in fluid phase is already a handled task and several different techniques have been developed for this purpose. One of them is based on measuring the projected area of a vesicle aspirated in a capillary (micropipette) as a function of the membrane tension; see e.g. (Needham and Zhelev 1996). The aspiration pressure defines the tension σ applied to the membrane. Measuring the relative area change in the regime of low tension, also known as 'entropic' tension (Helfrich and Servuss 1984, Evans and Rawicz 1990), allows for extracting the value of κ:

$$\frac{A - A_0}{A_0} \approx \frac{k_BT}{8\pi\kappa} \ln \sigma/\sigma_{in}. \tag{4}$$

Here A is the vesicle area at tension σ and A_0 is the initial area for which $\sigma = \sigma_{in}$. In this limit the aspiration pressure is very weak and the membrane is practically not dilated but only its undulations are flattened out. The real dilation occurs at tensions above $\sim$0.1 dyn cm^{-1} where the relative area change increases linearly with the membrane tension:

$$\frac{A - A_0}{A_0} \approx \frac{\sigma}{K_a}. \tag{5}$$

In this regime measuring the relative area change as a function of the membrane tension provides the stretching elasticity constant K_a, which is of the order of 200 dyn cm^{-1} for phosphatidylcholines in fluid phase (see table 1). Thus, from one measurement of the relative area expansion at various tensions one can extract both the bending rigidity and the stretching elasticity constants. The complete tension range is described by (see Evans and Rawicz 1990, Evans and Rawicz 1997, Rawicz *et al* 2000)

$$\frac{A - A_0}{A_0} = \frac{k_BT}{8\pi\kappa} \ln\left(1 + 0.1\frac{\sigma A}{\kappa}\right) + \frac{\sigma}{K_a}. \tag{6}$$

The micropipette technique for measuring the elastic constants is applicable to polymersomes as well. One example of data collected from vesicles made of the diblock copolymer PB_{32}–PEO_{20} is given in figure 4 (for details see Dimova *et al* (2002b)). The membrane tension, σ, is plotted versus the measured relative area change, $(A - A_0)/A_0$, for

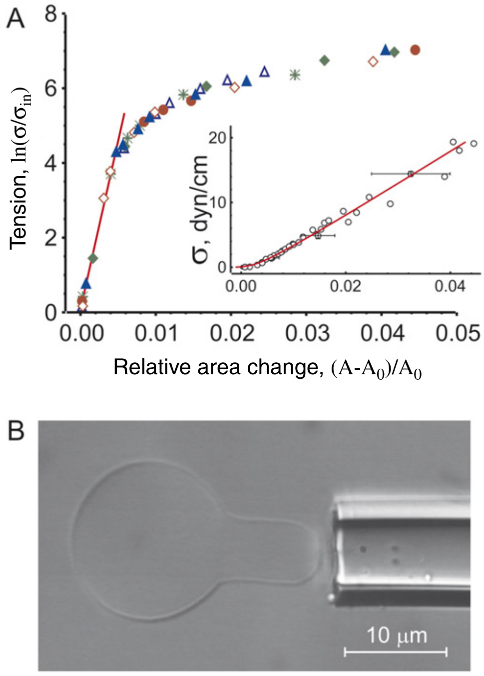

Figure 4. Micropipette manipulation of polymer vesicles. (A) Data from the relative area change of several vesicles (different symbols), adapted from (Dimova *et al* 2002b). In the entropic regime the slope of the solid line provides $\kappa = 42 \pm 5\ k_B T$, ($\sigma_{in} = 0.02$ dyn cm^{-1}). In the high tension regime the membrane stretching scales linearly with tension. The solid curve in the inset (same data) is a fit over the entire interval of tensions assuming a superposition of bending and stretching elasticities (see equation (6)), $K_a = 470 \pm 15$ dyn cm^{-1}. (B) A snapshot (differential interference contrast microscopy) of a polymersome a minute after it has been released from the pipette (also seen on the snapshot). The vesicle retains its shape for a few minutes because of the high viscosity of the membrane.

several vesicles. In the low tension regime the relative area change depends logarithmically on the tension and the proportionality factor gives κ. For the high tension regime the dependence is linear with a slope equal to K_a; see the inset in figure 4(A) and equation (5). The bending rigidity of these vesicles was found to be about 40 $k_B T$. This value is not unreasonably high and implies that when deformed by the pipette aspiration and subsequently released the vesicle should relax due to thermal noise. However, this relaxation is extremely slow, which is due to the high membrane viscosity of these polymersomes; see table 1. Thus, an aspirated vesicle keeps memories of its shape for several minutes after being released from the pipette; see figure 4(B).

From a conceptual point of view, one should distinguish two different tensions which are conjugate to the intrinsic and the projected area, respectively. Both tensions have been recently measured in molecular dynamics simulations and were found to be different in magnitude (Imparato *et al* 2005).

Another approach for measuring κ for lipid membranes consists of observing the shape fluctuations of a flaccid vesicle under the action of thermal agitation only (Méléard *et al* 1997). The analysis of the fluctuation modes allows estimating not only the bending rigidity but also the membrane spontaneous curvature (Döbereiner *et al* 1997, 2003). The experimental approach consists of acquiring a time sequence of contours of a fluctuating prolate vesicle. The contour is then presented in polar coordinates (R, φ) and expanded in Fourier series around the equivalent sphere radius, R_0, of the vesicle:

$$R(\varphi) = R_0 \left[1 + \sum_n a_n \cos(n\varphi) + \sum_n b_n \sin(n\varphi) \right]. \qquad (7)$$

The amplitudes $\{a_n, b_n\}$ are numerically calculated; see Döbereiner *et al* (1997). The membrane spontaneous curvature, M_{sp}, is proportional to the ratio of the mean square average values of the second and the third modes, $\langle a_2^2 \rangle$ and $\langle a_3^2 \rangle$, of the fluctuation spectra (Döbereiner 1995, Döbereiner *et al* 1997)

$$M_{\mathrm{sp}} \propto \langle a_3^2 \rangle / \langle a_2^2 \rangle \equiv \bar{M}_{\mathrm{sp}}. \qquad (8)$$

The dimensionless curvature ratio, $\bar{M}_{\mathrm{sp}}$, is determined directly from the statistics in the time sequence of the fluctuation modes. Evaluating the changes in the spontaneous curvature as estimated from fluctuation analysis was applied to vesicles subjected to transmembrane sugar asymmetry (Döbereiner *et al* 1999).

4.2. Curvature effects induced by polymer grafting

In general, the spontaneous curvature of GUVs is close to zero because on a micron-size scale the bilayer is symmetrical. However, in the presence of amphiphiles or ions which adsorb or incorporate in the external leaflet of the bilayer the spontaneous curvature can change drastically when the membrane accommodates the foreign molecules. In order to illustrate the change in the spontaneous curvature of a vesicle we will give two examples related to polymers anchoring or inserting in the bilayer.

First, we used vesicles containing biotinylated lipids. The vesicles were formed in the presence of the protein avidin. Because avidin has four sites for binding biotin groups the produced vesicles were covered with 'avidin anchor sites' which are able to trap biotinylated molecules from the solution. We used λ-phage DNA with one biotinylated end as long polymers to study the curvature change induced by anchoring of the molecules to the membrane (Nikolov *et al* 2004, Nikolov *et al* 2006). Curvature effects due to polymer grafting were theoretically addressed in previous studies (Hiergeist and Lipowsky 1996, Lipowsky 1995, Breidenich *et al* 2000). One example of the influence of anchoring of the DNA molecules onto the membrane is given in figure 5. The probability distributions of the second and first modes of the fluctuation spectra are given for a vesicle before and after subjecting it to the DNA solution. The vesicle is initially a prolate whose ellipticity is characterized by the mean value of a_2 (i.e. the position of the maximum in the histogram of a_2). After introducing the DNA solution, the histograms for the different shape modes change as the DNA molecules are anchored to the membrane. The widths of the two distributions which correspond to the mean square average values $\langle a_2^2 \rangle$ and $\langle a_3^2 \rangle$ decrease, with a significantly more pronounced effect on $\langle a_2^2 \rangle$. This implies that the curvature ratio $\bar{M}_{\mathrm{sp}}$ (see equation (8)) and, thus, the membrane spontaneous curvature, increase.

The second example for the change of the membrane spontaneous curvature is provided by insertion of oligooxyethylene alkyl ethers in lipid membranes (Dimova *et al* 2002a). These water soluble molecules are amphiphilic and have a hydrophobic anchor (hydrocarbon chain) connected to a hydrophilic part (oligoethyleneglycol). The effect of these amphiphiles on the membrane spontaneous curvature is again detected by monitoring the morphological response and fluctuation spectra of giant unilamellar vesicles exposed to a solution of the oligomer molecules (at a concentration below their critical micelle concentration). The time dependence of the curvature ratio $\bar{M}_{\mathrm{sp}}$ before and after introducing the amphiphile solution is given in figure 6. Interesting dynamics is observed. First the curvature ratio drastically

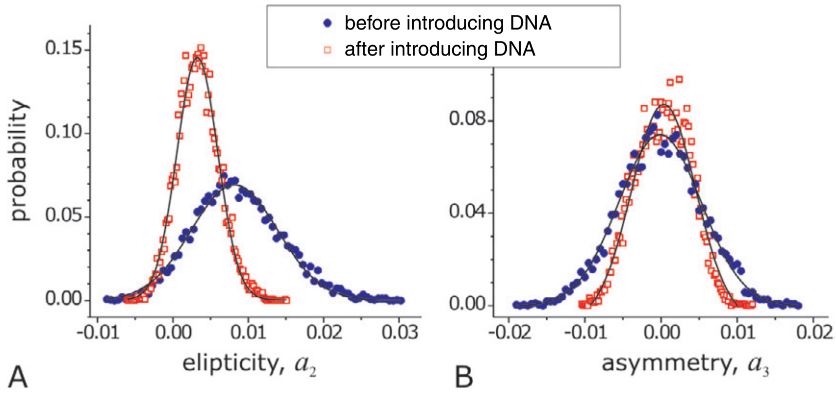

Figure 5. (A) and (B) exhibit normalized histograms for the mode amplitudes a_2 and a_3, respectively, for a prolate vesicle with avidin anchor sites in the absence and presence of biotinylated DNA. The DNA anchors to the membrane, which leads to a change in the membrane fluctuation spectrum as illustrated by the change in the mode distribution. The histogram statistics is done over about 7000 data points. The solid lines are Gaussian fits to the data.

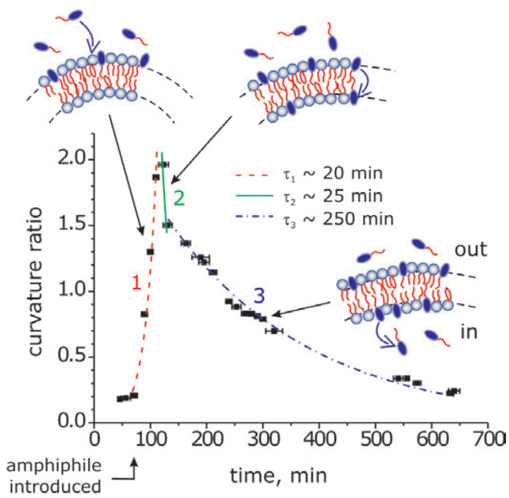

Figure 6. Time dependence of the curvature ratio $\bar{M}_{sp}$ (see equation (8)) of a vesicle subjected to a solution of oligooxyethylene alkyl ether ($C_{13}E_{10}$). After introducing the amphiphile (at time = 80 min) three stages are observed, as illustrated by the cartoons: (1) a drastic increase in the curvature ratio due to insertion of the molecules in the external leaflet of the membrane; (2) a quick decrease in $\bar{M}_{sp}$, presumably due to a fast flip-flop of the oligomers; and (3) a very slow relaxation process back to the initial membrane curvature which represents the approach to adsorption–desorption equilibrium between the internal leaflet and the vesicle interior. The characteristic times, τ_i, from exponential fits (see legend) describing the dynamics of each of these stages are given in the legend. They are determined with an accuracy of ±10 min, which is the average acquisition period for each data point.

increases because of the insertion of the amphiphiles in the external monolayer of the vesicle (the inserting molecules are schematically presented in the cartoons as having dark blue headgroups). The characteristic time of this insertion process, τ_1, is of the order of 20 min. Then a quick curvature relaxation is detected, most probably due to a redistribution of the inserted molecules (one possibility could be flip-flop or exchange of molecules between the two

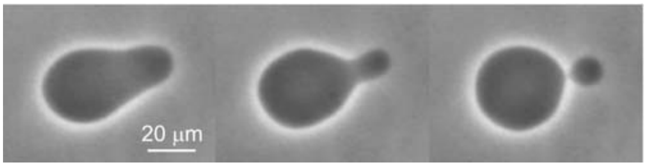

Figure 7. Snapshots of a budding vesicle (phase contrast microscopy). The vesicle has been subjected to a solution of amphiphilic molecules (same as in figure 6 but at higher concentration) which insert in the external leaflet of the membrane and induce a drastic increase in the spontaneous curvature. The vesicle volume is osmotically stabilized and remains constant. The complete budding event displayed in the snapshots takes place within about 5 s.

membrane leaflets through nanopores). Finally, a very slow relaxation process takes place with characteristic time, τ_3, of the order of 250 min. Presumably, this is the time needed to establish the adsorption–desorption equilibrium between the internal leaflet of the vesicle membrane and the encapsulated solution in the vesicle. The process establishes slowly, most probably because the adsorption rate is much larger than the desorption rate (as demonstrated by τ_1 and τ_3).

A more dramatic manifestation of the change in the spontaneous curvature can be exhibited in the evolution of the overall shape of the vesicle. For example, a prolate-to-oblate transition provides evidence for a decrease in the spontaneous curvature, while the so-called vesicle budding demonstrates an increase in the spontaneous curvature when the vesicle volume and area are conserved; see figure 7. During budding, the vesicle expels a small satellite vesicle or bud connected to the initial vesicle via a thin neck. In this case the spontaneous curvature of the system can be determined from the size of the bud (Seifert *et al* 1991).

5. Phase transitions in lipid bilayers

5.1. Bending rigidity of membranes in the gel phase

In the gel phase, the bending rigidity of single component lipid membranes is significantly larger than that of fluid membranes, and most of the classical methods for measuring κ mentioned in the previous section cannot be applied. Recently a few new methods have been developed for measuring the bending rigidity of membranes in the gel phase (Dimova *et al* 2000b, Lee *et al* 2001, Mecke *et al* 2003). For the first time the temperature dependence of κ of a membrane in the gel phase was measured using optical dynamometry (Dimova *et al* 2000b, Dimova and Pouligny 2006).

The method consists of attaching two latex microspheres of similar size to the (fluid) membrane of a giant vesicle by means of two optical tweezers. When the bilayer is brought to the gel phase, the particle motion is frozen. In typical experimental conditions the contact line of the membrane on the bead is small and the particles are located more to the outside of the vesicle (see figure 8(A)). Using two optical tweezers characterized by their trap stiffness, or the trapping constant k_{RP}, one applies a radiation pressure force, F_{RP}, to displace one of these particles in the membrane plane by a mobile trap while holding the other one in the potential well of an immobile or fixed trap. For particle–membrane configurations such as the one shown in figure 8(A), the main membrane deformation caused by the particle's displacement is bending (see figure 8(C)). The experiment leads to measuring an apparent membrane spring constant, k_{M} (Dimova *et al* 2000b). The relation between k_{M} and the membrane bending modulus, κ, is given by the empirical expression $k_{\mathrm{M}} \cong 60\kappa/a^2$, where a is the particle radius (Dimova *et al* 2000b). The bending rigidity of the membrane in the gel phase deduced in this way shows a considerable increase with lowering the temperature; see the open circles in figure 9. The data are presented as a function of the reduced temperature, $T - T_{\mathrm{m}}$, where T_{m} is the main phase

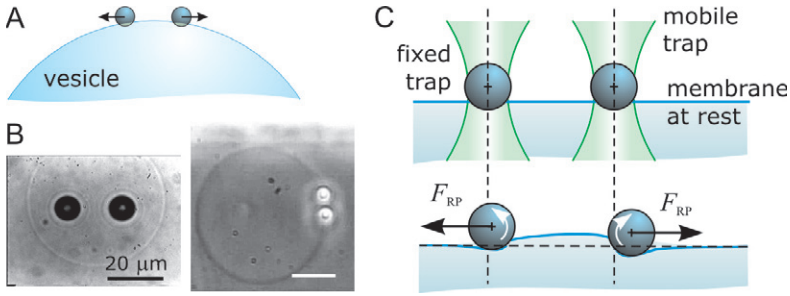

Figure 8. Optical dynamometry applied to measuring the bending rigidity of membranes in the gel phase. (A) Sketch of two particles adhering to the membrane of a vesicle. (B) Left: top view (in classical transmission microscopy) of two large particles located on top of a vesicle. The particles are about in focus. The image of the vesicle equator, well below the focal plane of the microscope, appears as clear faint ring. Right: two smaller particles are located at the vesicle equator. The scene is observed in phase contrast, providing a dark image of the membrane and bright images of the particles. (C) Sketch of the out-of-plane deformation of the membrane (side view) induced by pulling on one of the two particles and keeping the other one in the potential well of the fixed trap (optical traps are sketched in green). By measuring the relative displacement of both particles one can calculate the apparent spring constant of the membrane and subsequently determine the bending rigidity; see the open circles in figure 9.

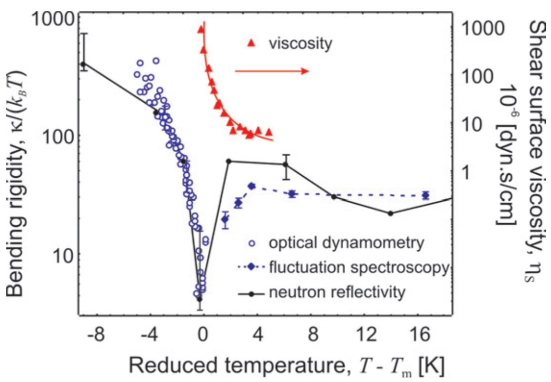

Figure 9. Bending rigidity (left axis) and shear surface viscosity (right axis) of a membrane undergoing its main phase transition. The bending modulus exhibits an anomalous decrease in the vicinity of the main phase transition temperature, T_m. Optical dynamometry data (adapted from Dimova *et al* (2000b)) (open circles) are collected for a membrane in the gel phase while fluctuation spectroscopy (adapted from Méléard *et al* (1997)) (solid (blue) diamonds) can be performed only when the membrane is in the fluid phase. The data from neutron reflectivity (adapted from Mecke *et al* (2003)) (dots and solid line) on floating bilayers in the vicinity of solid support span both phases. The membrane viscosity (solid (red) triangles; right axis) obtained from optical dynamometry (adapted from Dimova *et al* (2000b)) diverges as the membrane approaches T_m from the fluid phase. The solid (red) line is a fit to a power law: $\eta_S = 25\times10^{-6}|T - T_m|^{-1.4}$ dyn s cm^{-1}.

transition temperature of the lipid (this way of plotting allows for comparison of data for different lipids). This temperature dependence of κ was later confirmed by another technique based on neutron reflectivity (Fragneto *et al* 2001, Mecke *et al* 2003) (data displayed in figure 9) which can be applied to membranes both in the fluid and in the gel phase. The data show a pretransitional feature of critical decrease in the bending rigidity when T_m is approached, i.e. at zero reduced temperature. This anomaly in the behaviour of κ was predicted on the bases of analysis of heat capacity data from suspension of small vesicles (Heimburg 1998).

5.2. Shear surface viscosity measurements

To complete the property portrayal of a membrane crossing its main phase transition, we have complemented figure 9 with a set of data on the shear surface viscosity, η_S. The bilayer rheological properties were characterized using optical manipulation of a single particle attached to the membrane of a giant vesicle. Such particles were found to provide a sensitive tool for probing the state of the membrane. The Brownian trajectories of small beads can be used to extract their diffusion coefficient, D, which is inversely proportional to the friction coefficient, ζ, according to the Einstein relation, $D = k_B T/\zeta$. Measuring the sedimentation velocity of a large (heavy) particle shearing the membrane as it glides from the top to the bottom of a vesicle provides the friction coefficient. A third method for measuring ζ is related to following the displacement of a bead driven by the radiation pressure of an optical trap switched on in the particle vicinity. Extracting the membrane shear surface viscosity from the friction coefficient of a spherical bead straddling a membrane has already been theoretically treated in detail (Danov *et al* 2000, Dimova *et al* 2000a). The friction coefficient can approximately be decomposed into two terms:

$$\zeta = \zeta_0 + \zeta_m \tag{9}$$

where ζ_0 is the background or Stokes friction of the particle in the bulk solution, $\zeta_0 = 6\pi\eta a$, and ζ_m is the excess friction due to shearing the membrane. Here η is the viscosity of the surrounding fluid (the water solution) and a is the particle radius as introduced above. Similarly to the theory of Saffman for a disc shearing a membrane (Saffman and Delbrück 1975, Saffman 1976), the friction of the spherical particle due to the membrane was found to depend almost linearly on the membrane shear surface viscosity, η_S, and only weakly on the particle radius a:

$$\zeta_m \cong 2.93\eta_S \left(\frac{\eta a}{\eta_S}\right)^{0.12}. \tag{10}$$

In summary, using either thermal noise (Brownian motion), gravity (particle sedimentation) or the radiation pressure (optical dynamometry) as a driving force for the particle displacement, one can extract the friction coefficient of a bead attached to the membrane and respectively the shear surface viscosity of the membrane (Dimova *et al* 1999). Typical values for η_S are in the range 2–5 $\times$ 10^{-6} dyn s cm^{-1}. Note that the surface viscosity has units of [bulk viscosity $\times$ length] i.e. dyn s cm^{-1} (surface poises). To convert this value into some kind of a bulk viscosity of the lipid material one has to rescale it by the membrane thickness, $\sim$4 nm, which gives a bulk viscosity of the order of 5–10 dyn s cm^{-2} (poise) or 500–1000 times higher than water viscosity (10^{-2} dyn s cm^{-2}). This value is more than ten times higher than the bulk viscosity of alkanes (see e.g. Wakefield *et al* 1988, Queimada *et al* 2005) of length similar to the length of the fatty acid chains of lipids (e.g. 14–18 carbon atoms). This implies that with respect to their rheological properties lipid membranes cannot be considered as thin hydrocarbon films. Presumably, the membrane viscosity is different from the one of hydrocarbon melts because of the additional constraint on the displacement of the lipid chains imposed by the lipid headgroups.

Even though lipid bilayers are surprisingly viscous, the membrane friction is not the one dominating the resistance experienced by the particle shearing the membrane. Because the membrane is so thin compared to the particle size, the main dissipation occurs in the bulk solution. The contribution of the membrane friction when the bilayer is in the fluid state constitutes only some 30% of the total friction coefficient. This is not the case for polymer membranes. As already mentioned, diblock copolymer membranes exhibit a very high shear surface viscosity, $\eta_S \cong 1.5 \times 10^{-3}$ dyn s cm^{-1} (Dimova *et al* 2002b). Thus the effect of membrane resistance is significantly larger than the Stokes friction of the bead. The slow dynamics in the polymer membranes is obvious already when following the mobility of the latex probe attached to the membrane. While for a lipid vesicle in the fluid phase a bead of radius 5 μm takes about 2 min to span the pole-to-pole distance of a 50 μm vesicle, for a polymersome of similar size this time is longer than 2 h.

The lipid viscosity changes significantly at temperatures close to the main phase transition of the lipid. The shear surface viscosity of dimyristoylphosphatidylcholine membranes was found to increase a few orders of magnitude with decreasing the temperature (Dimova *et al* 2000b); see the data in figure 9. The drastic increase in η_S can be interpreted in terms of pretransitional structure fluctuations in the membrane. The fluid state is only defined as an average, so that a snapshot of the film at the molecular level would in fact reveal a mixture of fluid-like and gel-like domains as shown by computer simulations (Ipsen *et al* 1990, Jørgensen *et al* 1996).

To summarize, when approaching the main phase transition temperature the properties of the lipid bilayer change dramatically. Coming from the fluid phase and lowering the temperature causes an anomalous decrease in the bending rigidity of the membrane, while, simultaneously, the membrane viscosity exhibits a considerable increase as the membrane freezes. Other membrane properties like permeability (Cevc and Marsh 1987) and lipid flip-flop (John *et al* 2002) are also known to alter significantly when the membrane crosses the main phase transition temperature. In some particular cases (vesicles made of dimyristoylphosphatidylglycerol) the membrane perforates and cavities or pores of several nanometres in size are formed. This effectively turns the vesicle optically invisible upon cooling across the main phase transition temperature (Riske *et al* 2004a).

5.3. Multicomponent membranes

When multicomponent membranes are considered, the membranes can attain a larger variety of different states. At certain composition and/or temperature conditions, the membranes can be quenched into a phase coexistence region leading to the formation of domains of different characteristics (depending on their thermodynamic phase) on the same vesicle (Lipowsky and Dimova 2003). Solid domains tend to form facets or cylindrical segments whereas fluid domains tend to form spherical buds. Because the properties of the vesicle membrane vary locally a much larger assortment of vesicle shapes can be observed (Korlach *et al* 1999, Baumgart *et al* 2003). Recently, the studies on membrane domains have attracted significant scientific attention because of the relevance to the so-called rafts in biological membranes (Simons and Ikonen 1997). Even though giant vesicles, once again, have shown to be a very suitable and handy system to study the phase separation and domain formation in 'raft' mixtures (Dietrich *et al* 2001, Veatch and Keller 2003), the reader should be aware of the following concern. When giant vesicles are prepared from a multicomponent lipid mixture, the composition of the different vesicles in a batch can vary drastically depending on the individual history of the vesicles which is not known. For example, events like budding and pinching off of a part of the vesicle during the preparation and manipulation of the sample may lead to a vesicle composition totally different from the starting lipid mixture. An alternative and attractive way of arriving at a specific vesicle composition is to produce the domains starting from two vesicles made of different lipids and forcing them to fuse with each other, for example via electrofusion. An example of preliminary results from this procedure is given in figure 10. Two vesicles made of different lipids and labelled differently are subjected to a strong electric pulse and fuse. The resulting vesicle is made of two domains of the areas of which correspond to the sizes of the initial vesicles.

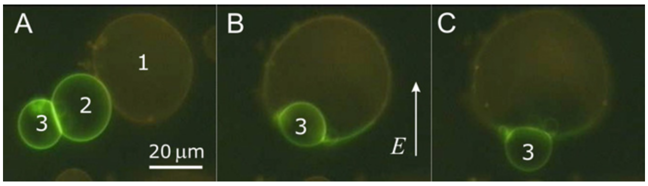

Figure 10. Electrofusion of vesicles with two different composition as observed with an optical microscope in fluorescence mode. (A) Two types of vesicle labelled with two fluorescent markers correspondingly. Vesicle 1 (larger vesicle in the right part of the snapshot) is made of dioleoylphosphatidylcholine (DOPC) with fluorescent probe DiIC18 (yellow). Vesicles 2 and 3 (two smaller vesicles adhering to each other in the left lower corner of the snapshot) are made of sphingomyelin:cholesterol (SPM:CHOL) in ratio 2:1 and are labelled with perylene (green). (B) The vesicles have been subjected to an electric pulse (6 kV cm^{-1}, 300 μs). The field direction is indicated with an arrow. The snapshot is taken several seconds after the pulse has been applied. Vesicle 2 has fused with vesicle 1 producing a brighter SPM:CHOL (green) domain in the lower part of the DOPC (yellow) vesicle (former vesicle 1). Vesicle 3 has not fused but only adheres to the larger vesicle. (C) A snapshot taken a minute later. The vesicle complex has slightly rotated and the adhesion area with vesicle 3 seems to have decreased. The SPM:CHOL (green) domain on the DOPC (yellow) vesicle is still visible.

Thus, starting with two (or more) domains produced by successive fusion one can address the question about the stability of such systems with respect to domain number and configuration. The excess area or reduced volume can then be controlled with a micropipette or by osmotic pressure varied from outside. Another interesting question, not yet addressed in the literature, is the effect of membrane tension on the domain stability. Increasing the membrane tension should influence the domain stability, presumably in a fashion similar to changing the temperature in the system.

6. Giant vesicles in electric fields

The interaction of electric fields with lipid membranes and cells has been extensively studied in the last decades (Neumann *et al* 1989, Chang *et al* 1992, Engelhardt *et al* 1984). In the presence of electric fields, lipid vesicles are deformed, because of the electric stress imposed on the lipid bilayer. The latter is given by the Maxwell stress tensor which can be used to calculate the membrane tension resulting from the electric field, i.e. 'electric' tension.

6.1. Vesicles in alternating electric (AC) fields

Subjected to AC fields, spherical vesicles assume elliptical shapes. The type and degree of deformation depends on several parameters, such as the field strength, E, and frequency, ω. The tension imposed by the AC field is usually in the entropic regime (see section 4.1) and results in pulling out the membrane undulations. Thus, shape analysis of elongated vesicles can be used to measure the bending rigidity of membranes (Kummrow and Helfrich 1991, Niggemann *et al* 1995). The tension acting on the membrane can be obtained from Kummrow and Helfrich (1991):

$$\sigma = \frac{9}{8}\varepsilon_0\varepsilon E^2 \frac{1}{(c_1+c_2)_{\mathrm{pole}} - (c_1+c_2)_{\mathrm{eq}}} \tag{11}$$

where ε is the dielectric constant of the aqueous solution, ε_0 the vacuum permittivity, and c_1 and c_2 are the principal curvatures of the membrane taken either at the equator (eq) or the

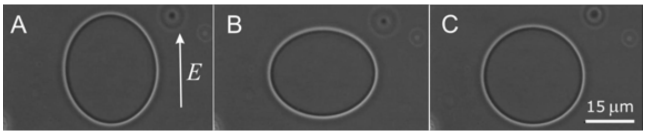

Figure 11. A giant vesicle (phase contrast microscopy) subjected to AC field of 0.2 kV cm^{-1}. The field direction is indicated with an arrow. The external solution is of conductivity higher than the internal one. From (A) to (C) the field frequency increases: (A) 5 kHz; (B) 100 kHz; (C) 10 MHz.

pole (pole) which are estimated from the microscopy images of the vesicle. The relative area change of the vesicle $(A - A_0)/A_0$ is measured and plotted as a function of the logarithm of the tension. Extrapolation to zero area change gives σ_{in} and the slope of the data provides the bending rigidity κ (see equation (4)). This method has been applied to vesicles in water which at intermediate field frequencies ($\omega = 2$ kHz) assume prolate deformation with the longer axis oriented in the field direction (Niggemann *et al* 1995). At higher frequencies (a few kHz) and again for vesicles in water medium a prolate–oblate transition is observed (Mitov *et al* 1993, Peterlin *et al* 2000) as theoretically predicted earlier (Hyuga *et al* 1991c, 1993).

It is interesting to note that non-spherical cells have been observed to *orient* parallel or perpendicular to the field (Zimmerman 1986), whereas, in a shape-analogous way, vesicles in water solutions *deform* with their largest cross section also being parallel or perpendicular to the field. The cell behaviour was found to depend on the medium conductivity conditions and field frequency (Iglesias *et al* 1985). To mimic a cell environment which is of conductivity much higher than that of pure water, we varied the salt concentration inside and outside the vesicle (Aranda *et al* 2006). When the solution inside the vesicle has conductivity lower than the external one, the vesicles attain a prolate deformation at low frequencies (less than several kHz) and oblate deformation at intermediate frequencies (up to several MHz); see figure 11. When the internal conductivity is higher, the prolate–oblate transition is not observed. At high frequency, more than about 10^7 Hz, the vesicles attain a spherical shape, irrespective of the conductivity conditions. Thus, by controlling the salt concentrations inside and outside a vesicle and scanning with the field frequency one can construct a morphological diagram depending on conductivity and frequency (Aranda *et al* 2006).

6.2. Vesicles subjected to electric pulses (DC fields)

When subjected to short and strong electric pulses ($\sim$100 μs, $\sim$1 kV cm^{-1}) the vesicle response is qualitatively similar to the one in AC fields. However, microscopy observation of effects caused by electric pulses on giant vesicles is difficult because of the short duration of the pulses. A possible solution to this problem is to slow down the vesicle response and relaxation by using a highly viscous solution, e.g. glycerin–water solution, as the medium instead of water (Sandre *et al* 1999). However, this trick affects the dynamics depending on the bulk viscosity of the solution but, supposedly, not the membrane dynamics which reflects the reorganization of the bilayer at shorter timescales. In addition, the presence of glycerin at high concentrations can lead to a change in the hydration of the lipids and correspondingly alter the membrane properties. Recently in our group, imaging with a fast digital camera was used to record the pulse response of giant lipid vesicles with a high temporal resolution of up to 30 000 frames s^{-1} (fps) (1 image every 33 μs) (Riske and Dimova 2005). One example of a vesicle deformation and poration is given in figure 12. This sequence clearly shows that imaging with a fast camera can reveal an essential part of the vesicle response which is not accessible to

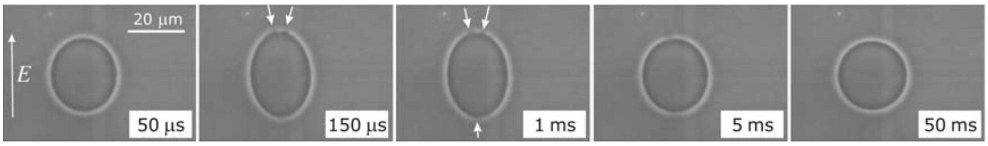

Figure 12. Selected snapshots from fast imaging of a giant vesicle (phase contrast microscopy; the internal solution is sucrose and the external one glucose; acquisition rate 20 000 fps). The vesicle is subjected to a DC pulse of duration 200 μs and strength 1.4 kV cm^{-1}. The direction of the field is shown in the first snapshot. The time indicated in the lower right corner of each snapshot is the time after the pulse has been applied. The spherical vesicle is forced to deform into a prolate with the long axis parallel to the field direction. The arrows in the second and third snapshots indicate pores ($\sim$ up to 4 μm in diameter) at the vesicle poles visualized by dark spikes of sucrose solution leaking out of the vesicle.

observation at standard video frequencies (at typical video frequency, $\sim$25 fps, the first three snapshots of figure 12 would be impossible to record, i.e. the information about the vesicle deformation and poration would be lost).

6.2.1. Electrodeformation. When subjected to a DC pulse, the transmembrane potential induced at the vesicle poles facing the electrodes, at time t is given by (Kinosita *et al* 1988):

$$V_m = 1.5RE(1 - e^{-t/\tau_{\text{charg}}}) \tag{12}$$

where R is the vesicle radius and τ_{charg} is the membrane charging time (Kinosita *et al* 1988):

$$\tau_{\text{charg}} = RC_m[1/\lambda_{\text{in}} + 1/(2\lambda_{\text{out}})]. \tag{13}$$

Here C_m is the membrane capacitance ($\sim$1 μF cm^{-2} for lipid membranes (Needham and Hochmuth 1989, Cevc 1993)), and λ_{in} and λ_{out} are the conductivities of the internal and external vesicle solution, respectively. For low conductivity solutions (a few μS cm^{-1}) and for a typical vesicle radius $R \sim 15$ μm, the membrane charging time $\tau_{\text{charg}} \sim 450$ μs. The created transmembrane potential V_m induces an effective electric tension σ_{el} (Abidor *et al* 1979, Needham and Hochmuth 1989):

$$\sigma_{\text{el}} = \varepsilon\varepsilon_0 \frac{h}{2h_e^2} V_m^2 \tag{14}$$

where h is the total bilayer thickness, ($\sim$4 nm), and h_e the dielectric thickness ($\sim$2.8 nm for lecithin bilayers (Simon and McIntosh 1986)). For vesicles with some initial tension σ_{in}, the final tension reached during the pulse is $\sigma = \sigma_{\text{in}} + \sigma_{\text{el}}$.

The overall deformation of a vesicle subjected to DC pulses corresponds to the shapes observed in the case of AC field, i.e. the vesicles assume prolate or oblate shape depending on the conductivity conditions, as discussed in section 6.1. Prolate and oblate deformations were theoretically predicted by Hyuga *et al* (1991b) and the response of the vesicle was treated as well. The experimentally observed relaxation dynamics (Riske and Dimova 2005) showed the presence of three regimes in the time dependence of the vesicle aspect ratio. At times of the order of a few hundred microseconds after the pulse, one observes area relaxation due to stretching and the characteristic time is $\sim\eta_S/\sigma$, where η_S is the surface viscosity of the bilayer as introduced above. At longer times, of the order of seconds, for vesicles with small reduced volumes ($v \leqslant 0.98$; see equation (1)), the vesicle dynamics is governed by curvature relaxation. The characteristic time is $\sim(4\pi\eta R^3/3\kappa)/(1/v - 1)$, where η is the bulk viscosity of sucrose/glucose solution, as above, R is the vesicle radius, and κ is the bending elasticity modulus of the membrane. An additional characteristic time describes the vesicle poration

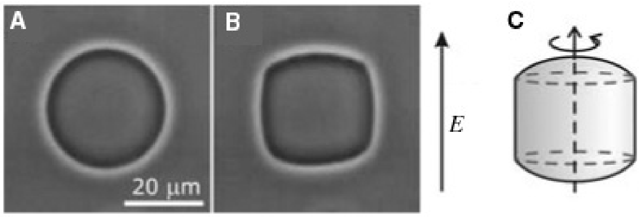

Figure 13. Vesicle response (observed with phase contrast microscopy) to an electric pulse of strength $E = 2$ kV cm^{-1} and duration 200 μs. The external solution contains 0.1 mM NaCl. (A) The vesicle is at rest before applying the pulse. (B) A snapshot of the vesicle 200 μs after the beginning of the pulse. The lifetime of this deformation is very short and of the order of few milliseconds. The direction of the field is indicated on the right. (C) A sketch of the approximate geometry of the vesicle: a cylinder with spherical caps. The deformed vesicle has an axial symmetry about the field axis.

(see section 6.2.2). In the theoretical studies treating the vesicle response to square-wave pulses (Hyuga *et al* 1991a, 1991b) the membrane stretching was ignored and only a qualitative agreement with the experimental data was found (Riske and Dimova 2005).

In the absence of salt in the vesicle exterior, the vesicles deform, assuming elliptical shapes as discussed above. But in the presence of salt, unusual shape transformations are observed (Riske *et al* 2004b, Riske and Dimova 2006). The vesicles assume cylindrical shapes with flat walls parallel to the field direction during the pulse. These deformations occur only in the presence of salt outside the vesicle, irrespective of their inner content. When the solution conductivities inside and outside are the same, vesicles with square-like cross section can be observed; see figure 13. The actual shape of the vesicle is a cylinder with spherical caps because of the axial symmetry about the field direction. These deformations are not equilibrium shapes and they have a very short life time, of the order of several hundred microseconds, which is why they cannot be observed at standard video frequency. As a possible explanation for the existence of these shapes one can consider the effective electrophoretic effect of the ions in the vesicle exterior (Riske and Dimova 2006).

6.2.2. Electroporation. When the vesicle tension reaches the so-called lysis tension, which is about 6 dyn cm^{-1} for phosphatidylcholine membranes (Needham and Hochmuth 1989), the membrane ruptures. The lysis tension of polymersomes is much higher, and exceeds 20 dyn cm^{-1} (Aranda-Espinoza *et al* 2001), which is why they are referred to as tough vesicles. In general, the lysis tension depends on the rate of stretching (Evans *et al* 2003). However, if one considers the stretching rate $d\sigma_{el}/dt$ as obtained from equations (14) and (12), one finds that this rate is relatively small and to a good approximation the lysis tension can be assumed close to the values mentioned above.

The phenomenon of membrane electroporation is of particular interest, because of its vast use in cell biology and biotechnology. Electroporation experiments on giant vesicles made of lipids and polymers are of special relevance because their size is comparable to that of cells and it allows for direct observation using optical microscopy (Zhelev and Needham 1993, Sandre *et al* 1999, Tekle *et al* 2001, Aranda-Espinoza *et al* 2001). The latter technique, however, can only detect pores which are larger than about half a micron. Macropores of a few micrometres in size induced by electroporation can be easily visualized especially when the sucrose/glucose refractive index asymmetry across the membrane is employed. When the vesicle is subjected to a short electric pulse and porates, the sucrose solution leaks through the macropores producing dark spikes on the vesicle image; see the second and third snapshots in figure 12. Detection of such spikes was used to characterize the electroporation of giant vesicles and analyse the characteristic time of pore closure (Riske and Dimova 2005). The resealing of the membrane occurs with a characteristic time of ~10 ms. The driving force for the process of pore closure is the edge tension of the pore that originates from the energetic cost to rearrange or curve the lipid molecules on the edge of the pore. The edge energy per unit length γ can be estimated to be $\kappa/2h$ and is of the order of 10^{-6} dyn (Harbich and Helfrich 1979). The characteristic time for pore closure (several milliseconds) is $\sim\eta_S r_{pore}/2\gamma$, where r_{pore} is the pore radius.

Electroporation is a necessary condition for the electrofusion of two vesicles in contact. Bringing two vesicles together can be achieved by applying AC fields. Similarly to cells, vesicles align to form pearl-chains in the field direction (Zimmerman 1986). Because poration occurs in the area of the vesicle poles facing the electrodes, the aligned vesicles porate in the area of their contact zone, which leads to fusion. Using a fast digital camera, the fusion dynamics has been observed with high temporal resolution (Riske *et al* 2004b, Haluska *et al* 2006). The fusion event consistently takes place at times shorter than 200 μs. Two regimes in the evolution of the fusion neck were observed related to molecular reorganization of the bilayers and hydrodynamics of fluid mixing of the vesicle contents.

7. Conclusion and perspectives

An important step for the understanding of the properties and functions of cell membranes is the characterization of lipid membranes. Giant vesicles provide a unique and particularly convenient system which allows for direct observation of the membrane response. In this paper we have reviewed work mainly done on vesicles in inert solutions or in the presence of amphiphiles. A large amount of research has also been done on vesicles in the presence of substances (reactants) which interact with the membrane and alter the membrane composition (one example is provided by enzymes; see Riske and Döbereiner (2003)). A simple way of studying such effects is by performing local injection of the reactant in the vicinity of a giant vesicle, or by exchanging the external solution of a vesicle by a slow flow of the reactant solution. In order to prevent osmotic inflation or deflation, all solutions have to be osmotically balanced with the vesicle solution.

One example of how simple microscopy observation on giant vesicles can give extensive information on the membrane response to ions is given in figure 14. A vesicle composed of neutral and negatively charged lipids is subjected to an isoosmolar solution of $CaCl_2$. Initially the vesicle fluctuates strongly, which is indicative of a low membrane tension. An isotonic solution of 7 mM $CaCl_2$ in glucose is then pumped into the vesicle chamber until the solution in the vesicle exterior has been completely exchanged (because of the glucose/sucrose asymmetry the solution inside the vesicles is somewhat denser than the external solution, and the vesicles are not washed out of the observation chamber while injecting the $CaCl_2$ solution). After several minutes, which is sufficient to establish a homogeneous concentration of $CaCl_2$ in the chamber, the fluctuations decrease continuously and stop (figure 14(B)). This indicates either an increase in the membrane tension or a stiffening of the membrane. Soon afterwards, the vesicle appears to lose and exchange fluid with the exterior (figure 14(C)). A strong indication for the vesicle volume exchange is that the internal glucose/sucrose contrast is lost. The hypothesis which best explains the observed dynamics and is supported by results from other techniques (Sinn *et al* 2006) is that the adsorption of the calcium ions causes condensation of the lipid molecules. Additional evidence for this proposal comes from the apparent thickening of the vesicle membrane (figure 14(C)). Thus, the ion adsorption seems to induce an effective

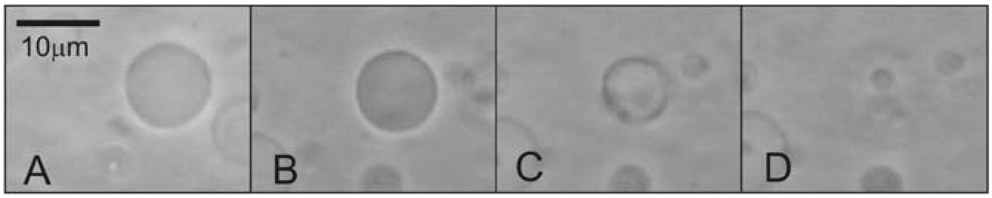

Figure 14. A sequence of pictures of a giant vesicle before and after introducing an isoosmolar solution of 7 mM $CaCl_2$ (adapted from Sinn *et al* (2006)). The complete event from (A) to (D) takes about 15 min, of which the transition from (B) to (D) takes about 2 min. The vesicle is composed of dioleoyl-phosphatidylcholine:dioleoyl-phosphatidylserine (1:5). (A) Before introducing the $CaCl_2$ solution the vesicle fluctuates strongly. (B) $CaCl_2$ solution has been injected and a significant decrease of fluctuations is observed. (C) The membrane appears thicker and the vesicle interior fades indicating leakage; the vesicle volume has also decreased. (D) The vesicle collapses and vanishes.

tension. The latter approaches the lysis tension of the membrane leading to poration and leakage (figure 14(C)), and finally, to membrane rupture and collapse (figure 14(D)).

The purpose of the sequence of snapshots discussed above is to demonstrate that simple microscopy observations on giant vesicles can reveal a large variety of events (in this case suppression of membrane fluctuations, leakage and bursting of a vesicle) induced by the interaction of ions or molecules with charged membranes. In a similar fashion, the direct microscopy observations on oligolamellar giant vesicles composed of palmitoyl-oleoyl-phosphatidylethanolamine and palmitoyl-oleoyl-phosphatidylglycerol (Pozo Navas *et al* 2005) were able to confirm the existence of unbinding transitions predicted earlier (Lipowsky and Leibler 1986).

In conclusion, giant vesicles are a simple and inspiring system which, without requiring sophisticated experimental equipment but just a microscope, can reveal the complex behaviour of membranes and answer fundamental questions about their interactions. Obviously, giant vesicles will continue to stimulate experiments that further improve our understanding of biomembranes.

Acknowledgment

RD is thankful to Hans-Günther Döbereiner for the instructive discussions on fluctuation analysis and for the collaboration on the project on insertion of amphiphiles in membranes. Cornelia Sinn is acknowledged for her work on adsorption of calcium on membranes and Thomas Franke for his work on vesicles adhering on adhesive substrates.

References

Abidor I G, Arakelyan V B, Chernomordik L V, Chizmadzhev Y A, Pastushenko V F and Tarasevich M B 1979 Electric breakdown of bilayer lipid membranes. I The main experimental facts and their qualitative discussion *J. Electroanal. Chem.* **104** 37–52

Abkarian M, Lartigue C and Viallat A 2001 Motion of phospholipidic vesicles along an inclined plane: sliding and rolling *Phys. Rev.* E **63** 1–7

Abkarian M and Viallat A 2005 Dynamics of vesicles in a wall-bounded shear flow *Biophys. J.* **89** 1055–66

Akashi K-I, Miyata H, Itoh H and Kinosita K Jr 1996 Preparation of giant liposomes in physiological conditions and their characterizations under an optical microscope *Biophys. J.* **71** 3242–50

Angelova M I and Dimitrov D S 1986 Liposome electroformation *Faraday Discuss. Chem. Soc.* **81** 303–11

Angelova M I, Soleau S, Méléard P, Faucon J-F and Bothorel P 1992 Preparation of giant vesicles by external AC electric fields. Kinetics and applications *Prog. Colloid Polym. Sci.* **89** 127–31

Aranda S, Riske K A, Lipowsky R and Dimova R 2006 Morphological phase diagram of frequency-dependent vesicle shapes induced by AC fields, in preparation

Aranda-Espinoza H, Bermudez H, Bates F S and Discher D E 2001 Electromechanical limits of polymersomes *Phys. Rev. Lett.* **20** 208301

Baumgart T, Hess S T and Webb W W 2003 Imaging coexisting fluid domains in biomembrane models coupling curvature and line tension *Nature* **425** 821–4

Boal D (ed) 2002 *Mechanics of the Cell* (Cambridge: University Press) p 159

Breidenich M, Netz R R and Lipowsky R 2000 The shape of polymer-decorated membranes *Europhys. Lett.* **49** 431–7

Brochard-Wyart F, de Gennes P G and Sandre O 2000 Transient pores in stretched vesicles: role of leak-out *Physica* A **278** 32–51

Cevc G (ed) 1993 *Phospholipids Handbook* (New York: Dekker)

Cevc G and Marsh D 1987 *Phospholipid Bilayers: Physical Principles and Models* ed E E Bittar (New York: Wiley)

Chang D C, Chassey B M, Saunders J A and Sowers A E (ed) 1992 *Guide to Electroporation and Electrofusion* (New York: Academic)

Danov K D, Dimova R and Pouligny B 2000 Viscous drag of a solid sphere straddling a spherical or flat surface *Phys. Fluids* **12** 2711–22

Davidson M W and Abramowitz M 1999 Optical microscopy, Online PDF resource micro.magnet.fsu.edu/primer/opticalmicroscopy.html

Dietrich C, Bagatolli L A, Volovyk Z N, Thompson N L, Levi M, Jacobson K and Gratton E 2001 Lipid rafts reconstituted in model membranes *Biophys. J.* **80** 1417–28

Dimova R, Danov K, Pouligny B and Ivanov I B 2000a Lateral motion of a large solid particle trapped in a thin liquid film *J. Colloid Interface Sci.* **226** 35–43

Dimova R, Dietrich C, Hadjiisky A, Danov K and Pouligny B 1999 Falling ball viscosimetry of giant vesicle membranes: finite-size effects *Eur. Phys. J.* B **12** 589–98

Dimova R, Döbereiner H-G and Lipowsky R 2002a Membrane curvature and dynamics induced by amphiphilic oligomers *Biophys. J.* **82** 506a

Dimova R and Pouligny B 2006 *Membrane Lipids* ed A Dopico (Totowa: Humana Press) at press

Dimova R, Pouligny B and Dietrich C 2000b Pretransitional effects in dimyristoylphosphatidylcholine vesicle membranes: optical dynamometry study *Biophys. J.* **79** 340–56

Dimova R, Seifert U, Pouligny B, Förster S and Döbereiner H-G 2002b Hyperviscous diblock copolymer vesicles *Eur. Phys. J.* B **7** 241–50

Discher B, Won Y-Y, Ege D, Lee J, Bates F, Discher D and Hammer D 1999 Polymersomes: tough vesicles made from diblock copolymers *Science* **284** 1143–6

Döbereiner H-G 1995 The budding transition of phospholipid vesicles: a quantitative study via phase contrast microscopy *PhD Thesis* Simon Fraser University, Canada, unpublished

Döbereiner H-G 2000 Properties of giant vesicles *Curr. Opin. Colloid Interface Sci.* **5** 256–63

Döbereiner H-G, Evans E, Kraus M, Seifert U and Wortis M 1997 Mapping vesicle shapes into the phase diagram: A comparison of experiment and theory *Phys. Rev.* E **55** 4458–74

Döbereiner H-G, Gompper G, Haluska C K, Kroll D M, Petrov P G and Riske K 2003 *Phys. Rev. Lett.* **91** 48301

Döbereiner H-G, Selchow O and Lipowsky R 1999 Spontaneous curvature of fluid vesicles induced by trans-bilayer sugar asymmetry *Eur. Biophys. J.* **28** 174–8

Engelhardt H, Gaub H and Sackmann E 1984 Viscoelastic properties of erythrocyte membranes in high-frequency electric fields *Nature* **307** 378–80

Estes D and Mayer M 2005 Giant liposomes in physiological buffer using electroformation in a flow chamber *Biochim. Biophys. Acta* **1712** 152–60

Evans E, Heinrich V, Ludwig F and Rawicz W 2003 Dynamic tension spectroscopy and strength of biomembranes *Biophys. J.* **85** 2342–50

Evans E and Rawicz W 1990 Entropy-driven tension and bending elasticity in condensed-fluid membranes *Phys. Rev. Lett.* **17** 2094–7

Evans E and Rawicz W 1997 Elasticity of 'fuzzy' biomembranes *Phys. Rev. Lett.* **79** 2379–82

Fischer A, Franco A and Oberholzer T 2002 Giant vesicles as microreactors for enzymatic mRNA synthesis *Chem. Biochem.* **3** 409–17

Fragneto G, Charitat T, Graner F, Mecke K, Périno-Gallice L and Bellet-Amalric E 2001 A fluid floating bilayer *Europhys. Lett.* **53** 100–6

Goetz R, Gompper G and Lipowsky R 1999 Mobility and elasticity of self-assembled membranes *Phys. Rev. Lett.* **82** 221–4

Gruhn T, Franke T, Dimova R and Lipowsky R 2006 Measuring the bending rigidity and adhesion energy of vesicles, submitted

John K, Schreiber S, Kubelt J, Herrmann A and Müller P 2002 Transbilayer movement of phospholipids at the main phase transition of lipid membranes: implications for rapid flip-flop in biological membranes *Biophys. J.* **83** 3315–23

Harbich W and Helfrich W 1979 Alignment and opening of giant lecithin vesicles by electric fields *Z. Naturf.* a **34** 1063–5

Haluska C K, Góźdź W T, Döbereiner H-G, Förster S and Gompper G 2002 Giant hexagonal superstructures in diblock-copolymer membranes *Phys. Rev. Lett.* **23** 238302

Haluska C K, Riske K A, Marchi-Artzner V, Lehn J-M, Lipowsky R and Dimova R 2006 Fusion in the fast lane: direct imaging of membrane fusion with high temporal resolution, submitted

Heimburg T 1998 Mechanical aspects of membrane thermodynamics. Estimation of the mechanical properties of lipid membranes close to the chain melting transition from calorimetry *Biochim. Biophys. Acta* **1415** 147–62

Helfrich M R, Mangeney-Slavin L K, Long M S, Djoko K Y and Keating C D 2002 Aqueous phase separation in giant vesicles *J. Am. Chem. Soc.* **124** 13374–5

Helfrich W and Servuss R M 1984 Undulations, steric interaction and cohesion of fluid membranes *Nuovo Cimento* D **3** 137–51

Henriksen J R and Ipsen J H 2002 Thermal undulations of quasi-spherical vesicles stabilized by gravity *Eur. Phys. J.* E **9** 365–74

Heuvingh J, Pincet F and Cribier S 2004 Hemifusion and fusion of giant vesicles induced by reduction of inter-membrane distance *Eur. Phys. J.* E **14** 269–76

Hiergeist C and Lipowsky R 1996 Elastic properties of polymer-decorated membranes *J. Physique* II **6** 1465–81

Hyuga H, Kinosita K Jr and Wakabayashi N 1991a Deformation of vesicles under the influence of strong electric fields *Japan J. Appl. Phys.* **30** 1141–8

Hyuga H, Kinosita K Jr and Wakabayashi N 1991b Deformation of vesicles under the influence of strong electric fields II *Japan J. Appl. Phys.* **30** 1333–5

Hyuga H, Kinosita K Jr and Wakabayashi N 1991c Transient and steady-state deformations of a vesicle with an insulating membrane in response to step-function of alternating electric fields *Japan. J. Appl. Phys.* **30** 2649–56

Hyuga H, Kinosita K Jr and Wakabayashi N 1993 Steady-state deformation of vesicle in alternating fields *Bioelectrochem. Bioenerg.* **32** 15–25

Iglesias F J, Lopes M C, Santamaria C and Dominguez A 1985 Orientation of schizosaccharomyces pombe nonliving cells under alternating uniform and nonuniform electric fields *Biophys. J.* **48** 712–26

Imparato A, Shillcock J C and Lipowsky R 2005 *Europhys. Lett.* **69** 650–6

Ipsen J H, Jorgensen K and Mouritsen O G 1990 Density fluctuations in saturated bilayers increase as the acyl-chain decreases *Biophys. J.* **58** 1099–107

Jørgensen K, Klinger A, Braiman M and Biltonen R L 1996 Slow nonequilibrium dynamical rearrangement of the lateral structure of a lipid membrane *J. Phys. Chem.* **100** 2766–9

Kinosita K Jr, Ashikawa I, Saita N, Yoshimura H, Itoh H, Nagayama K and Ikegami A 1988 Electroporation of cell membrane visualized under a pulsed-laser fluorescence microscope *Biophys. J.* **53** 1015–9

Korlach J, Schwille P, Webb W and Feigenson G 1999 Characterization of lipid bilayer phases by confocal microscopy and fluorescence correlation spectroscopy *Proc. Natl Acad. Sci. USA* **96** 8461–6

Kornberg R D and Mc Connell H M 1971 Inside-outside translocation of phospholipids in vesicle membranes *Biochemistry* **10** 1111–20

Kraus M, Seifert U and Lipowsky R 1995 Gravity-induced shape transformations of vesicles *Europhys. Lett.* **32** 431–6

Kummrow M and Helfrich W 1991 Deformation of giant lipid vesicles by electric fields *Phys. Rev.* A **44** 8356–60

Lee C-H, Lin W-C and Wang J 2001 All-optical measurements of the bending rigidity of lipid-vesicle membranes across structural phase transitions *Phys. Rev.* E **64** 020901

Lipowsky R 1991 The conformation of membranes *Nature* **349** 475–81

Lipowsky R 1995 Bending of membranes by anchored polymers *Europhys. Lett.* **30** 197–202

Lipowsky R 1999 *Statistical Mechanics of Biocomplexity* (*Lecture Notes in Physics* vol 527) ed D Reguera, J M Rubi and J M B Vilar (Berlin: Springer) pp 1–23

Lipowsky R and Dimova R 2003 Domains in membranes and vesicles *J. Phys.: Condens. Matter* **15** S31–45

Lipowsky R and Leibler S 1986 Unbinding transitions of interacting membranes *Phys. Rev. Lett.* **56** 2541–4

Long M S, Jones C D, Helfrich M R, Mangeney-Slavin L K and Keating C D 2005 Dynamic microcompartmentation in synthetic cells *Prog. Colloid Polym. Sci.* **102** 5920–5

Mecke K R, Charitat T and Graner F 2003 Fluctuating lipid bilayer in an arbitrary potential: theory and experimental determination of bending rigidity *Langmuir* **19** 2080–7

Méléard P, Gerbaud C, Pott T, Fernandes-Puente L, Bivas I, Mitov M, Dufourcq J and Bothorel P 1997 Bending elasticities of model membranes—influences of temperature and sterol content *Biophys. J.* **72** 2616–29

Merkel R, Sackmann E and Evans E 1989 Molecular friction and epitactic coupling between monolayers *J. Physique* **50** 1535–55

Michel M, Winterhalter M, Darbois L, Hemmerle J, Voegel J C, Schaaf P and Ball V 2004 Giant liposome microreactors for controlled production of calcium phosphate crystals *Langmuir* **20** 6127–33

Mitov M, Méléard P, Winterhalter M, Angelova M I and Bothorel P 1993 Electric-field-dependent thermal fluctuations of giant vesicles *Phys. Rev.* E **48** 628–31

Mutz M and Bensimon D 1991 Observation of toroidal vesicles *Phys. Rev.* A **43** 4525–7

Needham D and Evans E 1988 Structure and mechanical properties of giant lipid (DMPC) vesicle bilayers from 20 °C below to 10 °C above the liquid crystal-crystalline phase transition at 24 °C *Biochemistry* **27** 8261–9

Needham D and Hochmuth R M 1989 Electro-mechanical permeabilization of lipid vesicles. Role of membrane tension and compressibility *Biophys. J.* **55** 1001–9

Needham D and Zhelev D V 1996 *Vesicles* ed M Rossof (New York: Dekker) chapter 9 (The Mechanochemistry of Lipid Vesicles Examined by Micropipet Manipulation Techniques) pp 373–444

Neumann E, Sowers A and Jordan C (ed) 1989 *Electroporation and Electrofusion in Cell Biology* (New York: Plenum)

Niggemann G, Kummrow M and Helfrich W 1995 The bending rigidity of phosphatidylcholine bilayers: dependences on experimental method, sample cell sealing and temperature *J. Physique* II **5** 413–25

Nikolov V, Lipowsky R, Döbereiner H-G and Dimova R 2004 Changes in the membrane spontaneous curvature induced by grafting of long polymers *Biophys. J.* **86** 197a

Nikolov V, Lipowsky R and Dimova R 2006 Behaviour of giant vesicles with anchored DNA molecules, in preparation

Noireaux V and Libchaber A 2004 A vesicle bioreactor as a step toward an artificial cell assembly *Proc. Natl Acad. Sci.* **101** 17669–74

Peterlin P, Svetina S and Žekś B 2000 The frequency dependence of phospholipid vesicle shapes in an external electric field. Pflügers *Arch. Eur. J. Physiol.* **439** R139–140

Pozo Navas B, Lohner K, Deutsch G, Sevcsik E, Riske K A, Dimova R, Garidel P and Pabst G 2005 Composition dependence of aggregation form and mixing properties in a bacterial model membrane system *Biochem. Biophys. Acta* **1716** 40–8

Queimada A J, Marrucho I M, Coutinho J A P and Stenby E H 2005 Viscosity and liquid density of asymmetric n-alkane mixtures: measurement and modeling *Int. J. Thermophys.* **26** 47–61

Rädler J and Sackmann E 1993 Imaging optical thicknesses and separation distances of phospholipid vesicles at solid surfaces *J. Physique* II **3** 727–48

Rawicz W, Olbrich K C, McIntosh T, Needham D and Evans E 2000 Effect of chain length and unsaturation on elasticity of lipid bilayers *Biophys. J.* **79** 328–39

Reeves J P and Dowben R M 1969 Formation and properties of thin-walled phospholipid vesicles *J. Cell Physiol.* **73** 49–60

Riske K A, Amaral L Q, Döbereiner H-G and Lamy M T 2004a Mesoscopic structure in the chain-melting regime of anionic phospholipid vesicles: DMPG *Biophys. J.* **86** 3722–33

Riske K A and Dimova R 2005 Electro-deformation and poration of giant vesicles viewed with high temporal resolution *Biophys. J.* **88** 1143–55

Riske K A and Dimova R 2006 Cylindrical deformation of giant vesicles in salt solutions induced by electric pulses: Squaring the circle, in preparation

Riske K A and Döbereiner H-G 2003 Diacylglycerol-rich domain formation in giant stearoyl-oleoyl phosphatidylcholine vesicles driven by phospholipase C activity *Biophys. J.* **85** 2351–62

Riske K, Lipowsky R and Dimova R 2004b High temporal resolution of electro-poration, fusion and deformation of giant vesicles. ‘Squaring’ the vesicles *Biophys. J.* **86** 518a

Rodriguez N, Pincet F and Cribier S 2005 Giant vesicles formed by gentle hydration and electroformation: A comparison by fluorescence microscopy *Colloids Surf.* B **42** 125–30

Saffman P G 1976 Brownian motion in thin sheets of viscous fluid *J. Fluid Mech.* **73** 593–602

Saffman P G and Delbrück M 1975 Brownian motion in biological membranes *Proc. Natl Acad. Sci. USA* **72** 3111–3

Sandre O, Moreaux L and Brochard-Wyart F 1999 Dynamics of transient pores in stretched vesicles *Proc. Natl Acad. Sci. USA* **96** 10591–6

Seifert U 1997 Configurations of fluid membranes and vesicles *Adv. Phys.* **46** 13–137

Seifert U, Berndl K and Lipowsky R 1991 Shape transformations of vesicles: phase diagram for spontaneous-curvature and bilayer-coupling models *Phys. Rev.* A **44** 1182–202

Seifert U and Lipowsky R 1995 *Structure and Dynamics of Membranes* (*Handbook of Biological Physics* 1A) ed R Lipowsky and E Sackmann (Amsterdam: Elsevier) pp 403–63

Simon S A and McIntosh T J 1986 Depth of water penetration into bilayers *Methods Enzymol.* **127** 511–21

Simons K and Ikonen E 1997 Functional rafts in cell membranes *Nature* **387** 569–72

Sinn C, Antonietti M and Dimova R 2006 Binding of calcium to phosphatidyl-phosphoserine membranes *Colloid Surf. A* at press

Tekle E, Astumian R D, Friauf W A and Chock P B 2001 Asymmetric pore distribution and loss of membrane lipid in electroporated DOPC vesicles *Biophys. J.* **81** 960–8

Veatch S L and Keller S L 2003 Separation of liquid phases in giant vesicles of ternary mixtures of phospholipids and cholesterol *Biophys. J.* **85** 3074–83

Wakefield D L, Marsh K N and Zwolinski B J 1988 Viscosities of nonelectrolyte liquid mixtures. II. Binary and quaternary systems of some n-alkanes *Int. J. Thermophys.* **9** 47–59

Wintz W, Döbereiner H-G and Seifert U 1996 Starfish vesicles *Europhys. Lett.* **33** 403–8

Yamashita Y, Oka M, Tanaka T and Yamazaki M 2002 A new method for the preparation of giant liposomes in high salt concentrations and growth of protein microcrystals in them *Biochim. Biophys. Acta* **1561** 129–34

Zhelev D V and Needham D 1993 Tension-stabilized pores in giant vesicles: determination of pore size and pore line tension *Biochim. Biophys. Acta* **1147** 89–104

Zimmerman U 1986 Electrical breakdown, electropermeabilization and electrofusion *Rev. Physiol. Biochem. Pharmacol.* **105** 175–256